Self-Assembly of Nanoparticles in Three-Dimensions: Formation of Stalagmites†

Claudia G. Sztrum, Oded Hod, and Eran Rabani*

School of Chemistry, The Sackler Faculty of Exact Sciences, Tel Aviv University, Tel Aviv 69978, Israel

Received: November 2, 2004; In Final Form: December 5, 2004

We develop a coarse-grained lattice gas model to describe drying-mediated self-assembly of nanoparticles in three dimensions. Our model is an extension of the model developed by Rabani et al. [*Nature* **2003**, *426*, 271] in two dimensions. We show that when liquid evaporation occurs layer by layer and solvation forces are strong, the resulting morphologies agree well with the predictions of the 2D model. We discuss scenarios in which the full 3D treatment is necessary and predict the formation of nanostalagmites.

I. Introduction

The assembly of colloidal-prepared nanocrystals into well-defined ordered arrays is one of the most promising techniques currently developed for advanced materials. Currently, it is well established that metallic or semiconductor nanocrystals self-assemble to form 2D superlattices when the solvent is evaporated, provided that the size distribution of the nanocrystals is sufficiently narrow. This has been demonstrated for a wide variety of nanocrystals including gold,[1−4] silver,[5−8] cobalt,[9−11] copper,[12] cadmium selenide,[13−16] cadmium sulfide,[17,18] indium phosphate,[19] ferrite nanocrystals,[20] and more.

Understanding self-assembly of nanocrystals is also an important fundamental problem by itself. When a liquid containing nanocrystals evaporates, various interesting self-assembled phases may form.[15,21−24] The formation of these morphologies is governed by a subtle interplay of a variety of influences. One of the key factors that governs the controlled precipitation and self-assembly processes involves various interactions between nanocrystals,[25−30] substrates, and solvents. Other factors include the drying kinetics,[31,32] hydrodynamic effects,[33] and self-diffusion of the nanocrystals on the substrate.[16]

The theoretical study of self-assembly of nanocrystals has been limited mainly to the treatment of *equilibrium* phenomena.[4,34,35] Ohara et al.[34] showed that the self-assembly of gold nanocrystals cannot be described in terms of a simple hard-sphere model (in which the phase transition is entropy driven)[36] and that the self-organization during solvent evaporation is strongly affected by the van der Waals attractions between the particles. The interactions were described phenomenologically by a potential given by the Hamaker form.[37] Although the net long-range interaction potential between the gold particles was on the order or less than k_BT, a solution of polydisperse gold nanocrystals formed crystallized opals, signifying the fact that the size-dependent attraction between the nanocrystals is sufficient to induce size segregation and reversible superlattice formation.[34]

Gold nanocrystals deposited at the air−water interface were also found to form circular domains (2D disks) at low densities and stripes at higher densities.[8] These unique structures were interpreted as equilibrium phenomena governed by the competition between an attractive long-range potential and a longer ranged repulsion potential.[38−40] A generic model potential was used to simulate these structures, and it was shown that the competition between the long-range attraction and longer ranged repulsion is necessary to reproduce the observed patterns.[8]

While some evaporation-mediated assembly processes may be understood from the standpoint of thermodynamics,[22] the formation of assembled phases upon drying is, in general, an example of nonequilibrium self-assembly.[23,41,42] Substrate roughness, solvent dewetting, and convective flow can lead to very interesting nonequilibrium structures.[43−45] An example is the formation of mesoscopic rings and honeycomb nanocrystal networks.[43−46] Another example is the formation of disks, ribbons, and cracks recently observed by Brus and co-workers.[15,16,21] These experiments utilize a thin solution that contains semiconductor nanocrystals passivated by an organic surface ligand. The solution wets the surface of the substrate, effectively forming a two-dimensional film. Brus and co-workers analyzed the formation of the different structures based on a simple picture where the evaporation of the liquid is equivalent to a temperature quench, and the different morphologies were analyzed based on a spinodal decomposition picture.[47−49]

Recently, Rabani et al.[50] presented a coarse-grained lattice gas model of nanoparticle self-assembly that includes the dynamics of the evaporating solvent *explicitly*. Despite the fact that their model completely neglects the atomistic nature of the nanoparticles and their passivation layer,[51,52] it accounts for nearly all observed spatial and temporal patterns. In addition, the model also predicts network structures that have not yet been explored. Rabani et al. discuss two distinct mechanisms of ordering, corresponding to homogeneous and heterogeneous limits of the evaporation dynamics.[50] Their calculations show how different choices of solvent, nanoparticle size and identity, and thermodynamic state give rise to various morphologies observed experimentally.

The approach developed by Rabani et al.[50] is limited to treatment of the formation of 2D structures. In this paper we extend the model of Rabani et al. to treat drying-mediated self-assembly of nanoparticles in 3D. A similar approach has been developed recently by Chandler and co-workers for understanding the dynamics of the hydrophobic effect.[53−55] Our model is described in section II. Several questions regarding the validity of the original 2D model are discussed in section III. For example, we show that if solvent evaporation occurs gradually, layer-after-layer, the resulting self-assembled morphologies

† Part of the special issue "David Chandler Festschrift".

* To whom correspondence should be addressed.

10.1021/jp044994h CCC: $30.25
Published on Web 01/25/2005

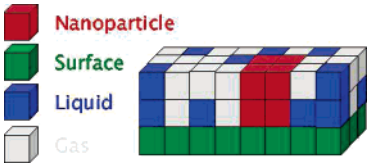

Figure 1. Sketch of the cubic lattice of our model. Each lattice cell of size ξ is occupied by gas, liquid, nanoparticle, or surface. The color scheme shown is maintained in subsequent figures.

simulated from the 3D model agree well with the predictions of the 2D model, given that nanoparticles are driven to the substrate by solvation forces. We further discuss scenarios where a 3D treatment is necessary and predict the formation of nanometer-scale stalagmites composed of nanoparticles. Finally, in section IV we conclude.

II. Model

The coarse-grained model we use to describe the self-assembly processes in 3D is an extension of the model developed by Rabani et al.[50] A sketch of the lattice is shown in Figure 1. The solvent and nanoparticles in our model are represented as a three-dimensional lattice gas.[56] Each cell of a cube lattice can be occupied by liquid or nanoparticle or vapor. The substrate (surface) is also modeled by a lattice gas. The size of each cell in the lattice equals the typical solvent correlation length, $\xi \approx 1$ nm. Because the size of a nanoparticle can exceed the range of correlated solvent fluctuations, we allow them to span several cells of the lattice, as can be seen in Figure 1. The lattice gas Hamiltonian can be expressed in terms of three binary variables, l_i, n_i, and s_i

$$H = -\epsilon_l \sum_{\langle ij \rangle} l_i l_j - \epsilon_n \sum_{\langle ij \rangle} n_i n_j - \epsilon_{nl} \sum_{\langle ij \rangle} n_i l_j - \epsilon_{ns} \sum_{\langle ij \rangle} n_i s_j - \epsilon_{ls} \sum_{\langle ij \rangle} l_i s_j - \mu \sum_i l_i \quad (1)$$

where l_i, n_i, and s_i are roughly proportional to the density of the solvent, nanoparticles, and substrate at lattice site i, respectively. Each binary variable can equal to 0 (low density) or 1 (high density); however, a single lattice site cannot be occupied by more than one species

The sum ($\sum_{\langle ij \rangle}$) in eq 1 includes only adjacent lattice cells. These cells attract one another with a strength that depends on the occupation of the two cells. The strength of the interactions between adjacent cells occupied by the liquid is determined by the energy density of the liquid and is given by ϵ_l. Similarly, when two adjacent cells are occupied by nanoparticles they attract one another with a strength determined by the nanoparticle interfacial energy given by ϵ_n. Adjacent cells that are occupied by different species also attract one another. The strength of nanoparticle−liquid, nanoparticle−substrate, and liquid−substrate attractions are given by ϵ_{nl}, ϵ_{ns}, and ϵ_{ls}, respectively. Since the value of the substrate binary variables is fixed in the simulations reported below, we exclude the constant term $\epsilon_s \sum_{\langle ij \rangle} s_i s_j$ from the Hamiltonian.

The last term on the right-hand side of eq 1 includes the solvent chemical potential, μ, which is used to establish the average concentration of liquid and vapor cells at equilibrium. A large negative value of μ will favor evaporation, while positive values will favor wetting. Since the vapor pressure of the nanoparticles and the substrate is negligibly small, we do not include a chemical potential for these species in the Hamiltonian. In other words, the binary variables associated with the nanoparticles and the substrate (n_i and s_i, respectively) conserve the corresponding densities (conserved order parameter), while the binary variable representing the liquid does not conserve density (nonconserved order parameter).[49]

The number of cells in each dimension is given by m_α with $\alpha = x, y, z$. An experimental realization of a thin film of nanoparticles deposited on a substrate is described by large values of m_x and m_y, typically several hundreds to thousands of cells representing a layer of several micrometers square in area. The z direction describes the height of the wetting layer. We take m_z to be on the order of several tens of nanometers (i.e., several tens of cells). We assume periodic boundary conditions in the $x-y$ plane only.

Initially, the lattice is entirely filled with liquid and nanoparticles, except for the first layer that is entirely filled with substrate cells. This lower layer is the only immobile layer, namely, the value of the cells in the lower layer is fixed for the entire simulation. Initially, nanoparticles acquire random position inside the simulation box. We fix μ at a value for which the equilibrium state is vapor and follow the dynamics of nanoparticle assembly coupled to the dynamics of the solvent evaporation.

The dynamics of our model are stochastic, both for fluctuations in solvent density and for nanoparticle diffusion. In the former case, configurations evolve by Monte Carlo dynamics. We attempt to convert a randomly chosen lattice cell i that is not occupied by a nanoparticle or the substrate, from liquid to vapor (or vice versa), $l_i \rightarrow (1 - l_i)$. In the case that $l_i = 1$, we attempt such a move only if $\sum_j (l_j + n_j + s_j) = 0$, where the sum runs over all lattice sites with the same x and y coordinate in the layers above site i. In other words, only if the cells above cell i are empty we attempt such a move. In the case that $l_i = 0$, we attempt such a move only if the lattice cell below is occupied by liquid, nanoparticle, or substrate. These moves are then accepted with a Metropolis probability, $p_{acc} = \min[1, \exp(-\Delta H/k_B T)]$, where k_B is the Boltzmann constant and ΔH is the resulting change in energy computed using the Hamiltonian given by eq 1. The main motivation to use this set of constraints on the liquid moves, which is different from the set of moves used by Chandler and co-workers,[53−55] is to avoid unphysical situations in which nanoparticles are surrounded by vapor (away from the substrate) in the limit of rapid evaporation. In this move the dynamics do not conserve solvent density within the film, as seems appropriate for an evaporating thin film solution.

As mentioned before, the nanoparticles have negligible vapor pressure, and therefore, their density should be conserved. Thus, in our model they execute a random walk on the three-dimensional lattice, biased by their interactions with each other, with liquid cells, and with the substrate. Specifically, we attempt to displace a nanoparticle by a single lattice spacing in a randomly chosen direction. Such a move is accepted with the same Metropolis probability but *only if* the region into which the nanoparticle moves is completely filled with liquid. Solvent density in lattice cells overtaken by this displacement is regenerated in the wake of the moving nanoparticle. This final constraint mimics the very low mobility of nanocrystals on a dry surface.[16] It also provides an additional coupling between the kinetics of evaporation and nanoparticle phase separation.[50]

In all the results reported below a single Monte Carlo step consists of an attempt to change the value of all liquid/vapor cells (note that the sum of liquid and vapor cells is conserved) followed by N_{move} attempts to move all nanoparticles. Thus, the diffusion rate of the nanoparticles is controlled by changing the value of N_{move}.

III. Results

In a typical self-assembly experiment the interactions between nanoparticles are screened by the solvent, such that self-organization of nanoparticles occurs when the solvent evaporates.[4] A realization of this experimental situation is achieved by carefully selecting the ratio between the solvent−solvent, solvent−nanoparticle, and nanoparticle−nanoparticle interaction strengths. Thus, in the first set of simulations we have chosen (in units of ϵ_l) $\epsilon_{nl} = 1.5$ and $\epsilon_n = 2$. The values of ϵ_{ls} and ϵ_{ns} determine the liquid−substrate and nanoparticle−substrate interface energy, respectively. The substrate will remain dry (wet) for small (large) values of ϵ_{ls}. Similarly, before the solvent evaporates nanoparticles will stick to the substrate for large values of ϵ_{ns} or remain solvated for small values of ϵ_{ns}. Below we discuss the effect of the substrate energetics on the resulting self-assembled structures.

We consider nonequilibrium initial conditions appropriate for experiments conducted in a closed chamber.[21] We assume that the initial configuration of nanoparticles with a given density ρ_n is random on the 3D lattice and all other cells that are not occupied by the substrate are filled initially with liquid. However, μ is fixed at a value for which the equilibrium state is vapor. For the present 3D model this occurs when $\mu < -3\epsilon_l$. The values of the chemical potential μ and the temperature T not only determine the average concentration of liquid and vapor cells at equilibrium but also strongly affect the dynamics of evaporation. When the solvent is near the spinodal limit of metastability, $\mu \approx \mu_{sp}(T)$, evaporation is spatially *homogeneous*.[50] Between binodal and spinodal lines, $-3\epsilon_l > \mu > \mu_{sp}(T)$, evaporation is instead strongly heterogeneous in space.[50] The transition between these limits of evaporation can be tuned by changing μ or T and is also discussed below.

One of the differences between the present 3D model and the 2D model developed by Rabani et al.[50] is the scaling of the nanoparticle interactions with size. It is well known that dispersion interactions between spherical particles scale linearly with size.[27] This behavior is well captured by the 2D model.[50] However, for the present 3D model these interactions scale with the surface area of the nanoparticles and not with their diameter. Therefore, caution must be taken when the results are compared for different size nanoparticles. In all applications reported below we assume that the size of nanoparticles is $2 \times 2 \times 2$ lattice cells. With proper parameter scaling[57] we find that the results are independent of the nanoparticle size, in agreement with experiments.[21] The size of the simulation box is $256 \times 256 \times 11$ with periodic boundary conditions in the $x-y$ plane. Since the lower layer is filled with substrate, nanoparticle and liquid can fill the top 10 layers only.

In Figure 2 we plot snapshots of the 3D simulated structures at different times with $\mu = -3.125$, $T = 0.5$, $\epsilon_{ls} = 1$, and $\epsilon_{ns} = 1.5$ (in units of ϵ_l). The 2D nanoparticle coverage is 0.4. For these conditions evaporation is homogeneous in space, the solvent does not wet the substrate at equilibrium (see right panels at long times), and nanoparticles do not stick to the substrate before the solvent evaporates. Left panels show the 3D nanoparticle density computed from a representative trajectory. Right panels show the corresponding density including that of the liquid. We find that at all times the liquid wets the interface of the nanoparticle domains.

At early times ($t = 1$, in units of Monte Carlo steps) nanoparticles fill random cells in the simulation box. The remaining cells are filled with liquid. The evolution of this nonequilibrium initial state toward equilibrium is driven by the value of the chemical potential, which favors evaporation.

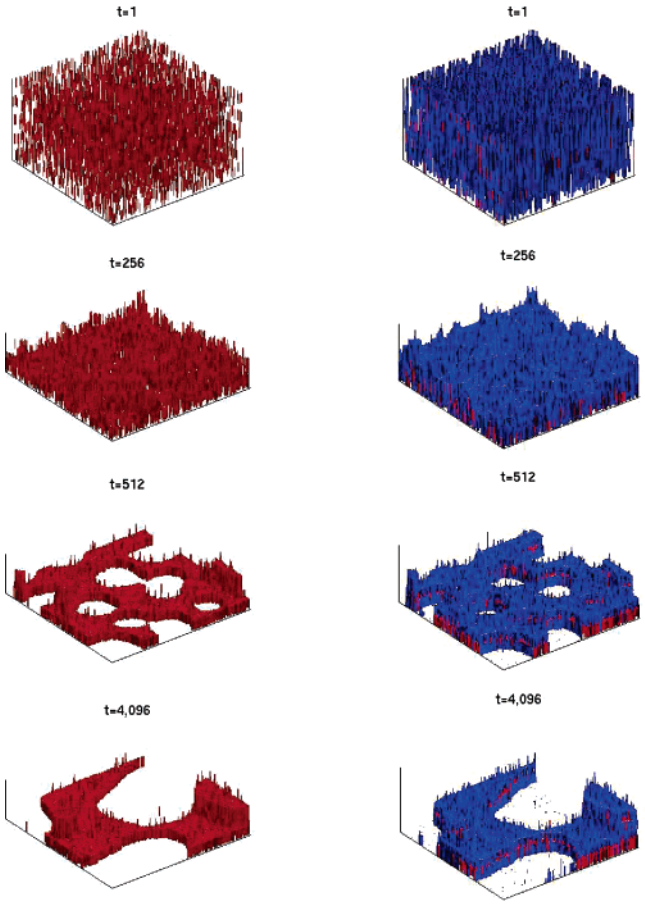

Figure 2. Snapshots of a 3D trajectory resulting from homogeneous evaporation and wetting of nanoparticle domains. (Left) Density of nanoparticles only (red), and (right) density of nanoparticles and density of the liquid (blue). Note the final structure is 2D with a small density of nanoparticles in the second layer.

Evaporation occurs layer by layer, and solvation forces drive the nanoparticles in the direction of the substrate. At intermediate times ($t = 256$) a thin *wet* layer of disordered nanoparticles is formed. Eventually, long wavelength fluctuations of the liquid density lead to the evaporation of the thin liquid layer and nanoparticles assemble to form ordered 2D arrays that are similar to the structures predicted using the 2D model.[50]

Most of the structures obtained in this limit have a small second layer, similar to the experimental observation.[15] The size of the second layer depends mainly on ϵ_{nl}, ϵ_{ns}, and ϵ_n. It diminishes for smaller interparticle interactions (ϵ_n) or larger nanoparticle−substrate interactions (ϵ_{ns}). We find that the size of the second layer may vary with time when the boundary of the nanoparticle domains remains fluxional throughout the growth dynamics. The latter condition requires that the boundaries are wet (i.e., covered with solvent) and that the energetic cost of moving a nanoparticle into the surrounding solvent is comparable to k_BT.

The above 3D self-assembly process can be described as a two-step process. This is best illustrated in Figure 3, where we plot the time evolution of the density of nanoparticles (bottom) and solvent (top) for each layer separately. The results are shown for the same trajectory as in Figure 2. At early times ($t < 256$) the solvent disappears gradually, layer after layer. Since the energy required to convert a liquid cell to vapor at the liquid/vapor interface is smaller than the bulk, the evaporation occurs in steps. Namely, evaporation in a given layer is triggered by the drying of the layer above. The solvent evaporation is

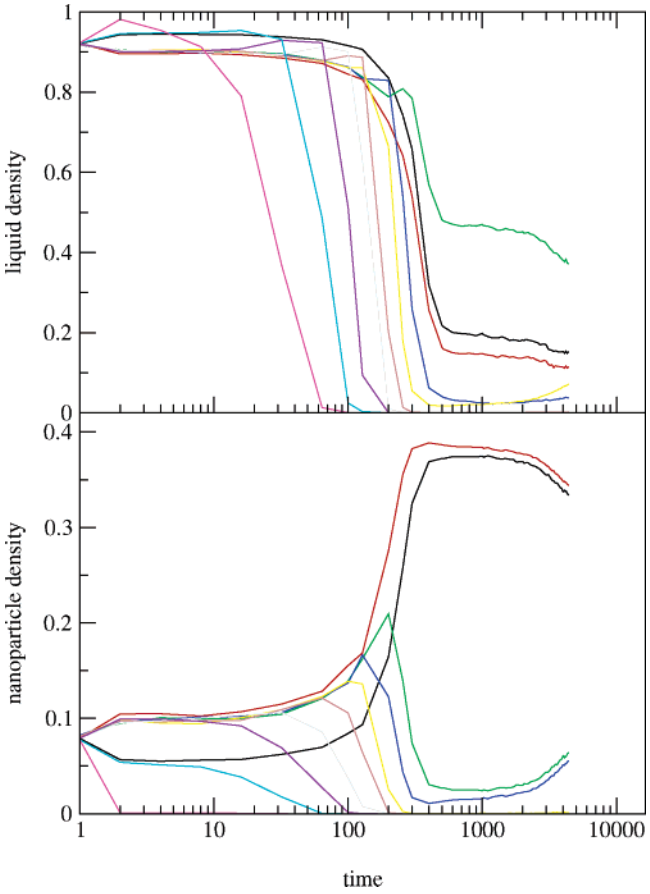

Figure 3. Time evolution of the density of nanoparticles (bottom) and liquid (top) for homogeneous evaporating conditions. Each color represents the time evolution of the 2D density at a different layer. The value of the 2D density is 1 if all cells are occupied or 0 if all cells are empty. Different curves represent the 2D density from bottom (near the substrate) to top: Black, red, green, blue, yellow, brown, gray, violet, cyan, and magenta. This color scheme is maintained in similar subsequent figures.

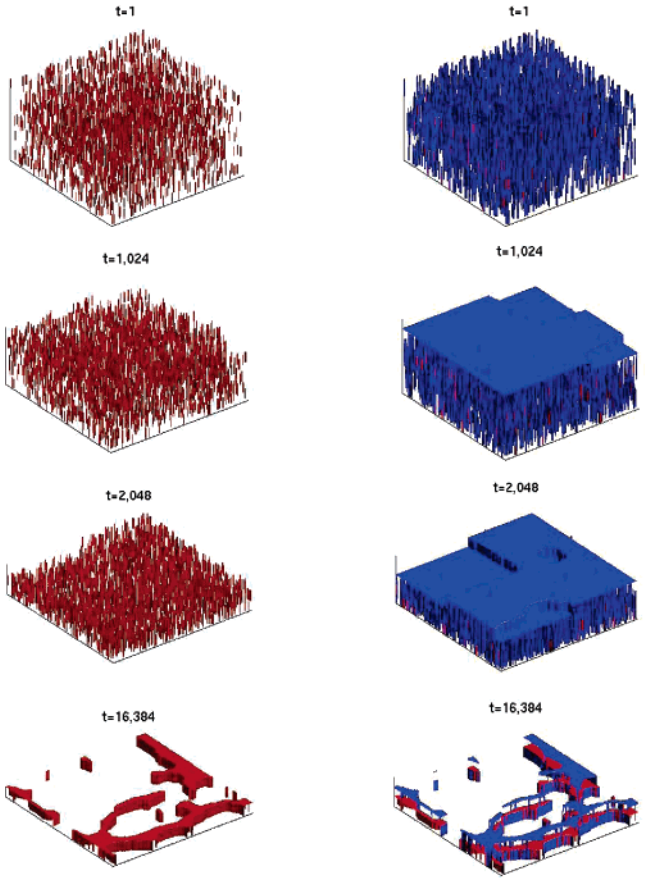

Figure 4. Snapshots of a 3D trajectory resulting from heterogeneous evaporation. (Left) Density of nanoparticles only (red), and (right) density of nanoparticles and density of the liquid (blue). Note that the final morphology is 2D. Under these conditions the density of nanoparticles in the second layer vanishes.

correlated with the increase of nanoparticle density near the substrate due to strong solvation forces. Effectively, a disordered thin layer of liquid and nanoparticles is formed. At longer times ($t > 300$) the remaining thin liquid layer evaporates, triggering the self-organization of nanoparticles into 2D ordered arrays. The growth dynamics and scaling laws of this second step are well captured by the simple 2D model of Rabani et al.[50] Naturally, the 2D model lacks the description of the formation of additional layers on top of the dominant lower layer nor can the 2D model describe the growth kinetics of nanoparticles in higher layers, as can be seen in the lower panel of Figure 3 at long times.

We also simulated the system under similar conditions in which the solvent evaporates gradually, layer by layer; however, the evaporation is instead strongly heterogeneous in space. As mentioned before, this is achieved by changing the chemical potential and/or the temperature. A snapshot of a typical trajectory under heterogeneous evaporation conditions is shown in Figure 4. These results were obtained for the same model parameters used for Figure 2 at a thermodynamic state corresponding to $\mu = -3.25$ and $T = 0.25$ (in units ϵ_1). Here, the 2D nanoparticle coverage is 0.2.

At early times ($t = 1$) nanoparticles fill random cells in the simulation box. The remaining cells are filled with liquid. Similar to the homogeneous evaporation limit, the evolution of this nonequilibrium initial state toward equilibrium occurs layer after layer. In this gradual process the nanoparticles are driven toward the substrate by solvation forces. Each solvent layer evaporates heterogeneously in space. Evaporation at the layer beneath is triggered when the liquid density above is very small. This is clearly seen in Figure 5, where we plot the time evolution of the density of the liquid (top) and the nanoparticles (bottom) for each layer separately. Note that the time scale for evaporation is much slower than the corresponding time scale in the homogeneous evaporation limit (see Figure 3 for comparison). At intermediate times ($t \approx 2000$) a thin layer of liquid and nanoparticles is formed. Eventually this thin layer of solvent will evaporate by nucleation and growth of vapor bubbles (and not by long wavelength fluctuations).[50] If nanoparticles are sufficiently mobile to track the fronts of growing vapor nuclei, their aggregate patterns will be shaped by the structural history of evaporation of the thin layer of solvent. The locations of nanoparticle domains at long times roughly traces the intersection lines of colliding vapor nuclei, leading to 2D network-like morphologies, similar to the morphologies obtained by Rabani et al. for the 2D model.[50] The resulting morphologies in this limit are a direct consequence of the coupling between two phase transitions, one in solvent density and the other in nanoparticle density.

Despite the fact that the dynamics of self-assembly in the heterogeneous evaporation limit are dramatically different, we find that as long as the evaporation kinetics is slower than the particle aggregation and solvation forces drive the nanoparticles toward the substrate, the resulting morphologies and characteristic time scales are well captured by the 2D model of Rabani

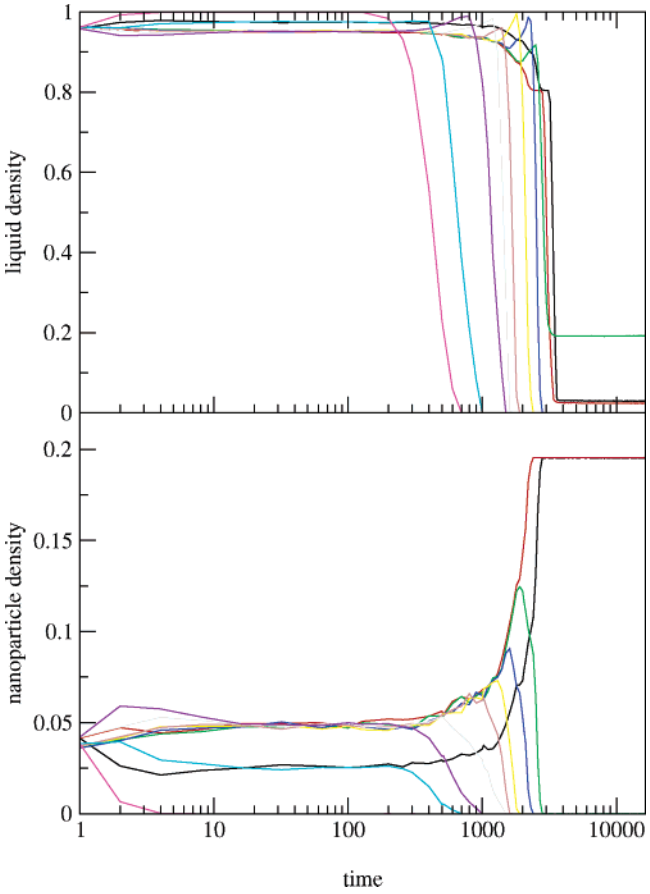

Figure 5. Time evolution of the density of nanoparticles (bottom) and liquid (top) for heterogeneous evaporating conditions. Each color represents the time evolution of the 2D density at a different layer. Color scheme same as in Figure 3.

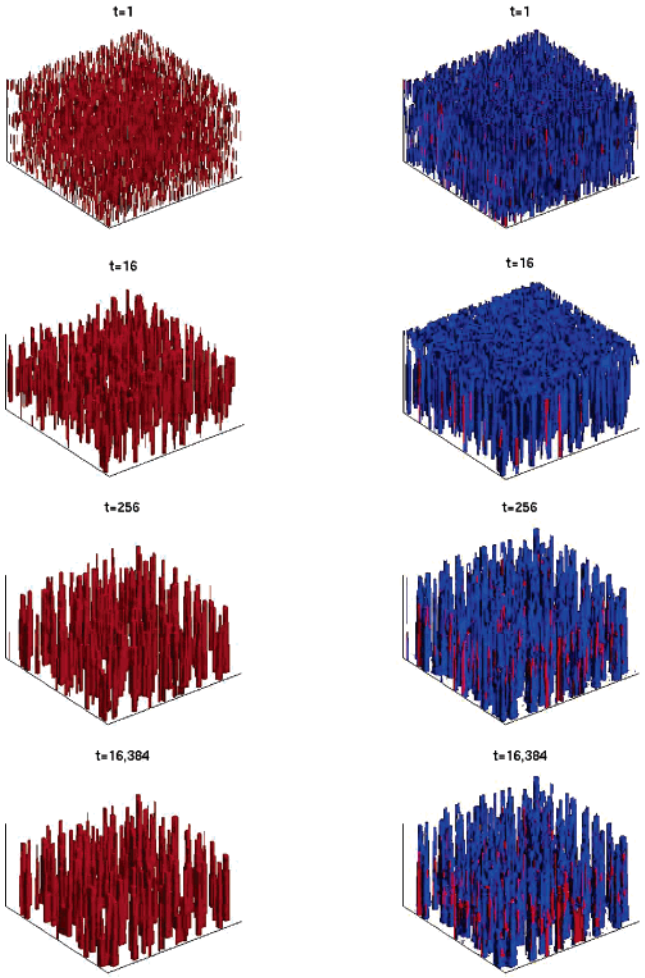

Figure 6. Snapshots of a 3D trajectory resulting from homogeneous evaporation. (Left) Density of nanoparticles only (red), and (right) density of nanoparticles and density of the liquid (blue). The formation of conical nanostalagmites seen at late times is a result of the increase of the interparticle interaction strength at $t = 0$.

et al.[50] This is true regardless of whether the solvent evaporated homogeneously or heterogeneous in space.

Thus far we have discussed the formation of 2D self-assembled morphologies. These 2D structures result from large solvation forces that drive the nanoparticles toward the substrate when the liquid evaporates. The large liquid interfacial energy leads to gradual evaporation that occurs layer by layer. Several pathways exist to form 3D self-assembled structures. One possible route is based on the reduction of the liquid interfacial energy. For example, density fluctuations near a critical point may lead to the formation of interesting 3D self-assembled structures governed by the long wavelength fluctuations of the solvent. Here, we have taken an alternative route, namely, at a given instant we increase the nanoparticle−nanoparticle interaction strength relative to that of the liquid−liquid interaction strength. This can be achieved experimentally by adding small amounts of a cosolvent with respect to which the nanoparticles are solvophobic[27] or by optically exciting the nanoparticles, thereby increasing their attractions.

In Figure 6 we show 3D snapshots of a typical trajectory following the above scenario. The thermodynamic state and model parameters are the same as those used in Figure 2. At $t = 0$ we increase the nanoparticle−nanoparticle interaction strength by 25%, namely, we increase ϵ_n from 2 to 2.5 (in units of ϵ_l). The liquid screens the interparticle interactions for $\epsilon_n = 2$ but not for $\epsilon_n = 2.5$. As a result the nanoparticles begin to aggregate and flocculate. This aggregation is strongly coupled to the dynamics of the evaporating liquid, since, as mentioned above, in our model a nanoparticle can diffuse randomly only if the region into which the nanoparticle moves is completely filled with liquid. As the solvent dries, the nanoparticles are pinned to their location and the growth of the domains nearly stops. Eventually we obtain a 3D structure of nanostalagmites. Despite the fact that the interface of the stalagmites is still wet (see right panels of Figure 6), the growth kinetic slows down considerably upon drying. Domain walls are only slightly fluxional since the energetic cost of moving a nanoparticle into the surrounding solvent is large compared to k_BT due to the increase in ϵ_n.

We find that the shape of the stalagmites is conical. The size of the base of the cones depends mainly on the diffusion rate of the nanoparticles. The formation of conical stalagmites is consistent with the result shown in Figure 7 for the time evolution of the density of nanoparticles (bottom) and liquid (top). The concentration of nanoparticles is larger closer to the substrate and decreases monotonically from the substrate.

The rate of growth of the stalagmites domains is correlated with the evaporation of the liquid, as clearly can be seen in the figure. A significant slowing down is observed at $t > 200$, where the liquid fills the lattice cells only at the interface of the nanoparticle domains. At long times reorganization of nanoparticle domains is driven by the reduction of interfacial energy of these domains. This explains the longer time decay of the liquid density, since the interfacial area of nanoparticle domains decreases with time.

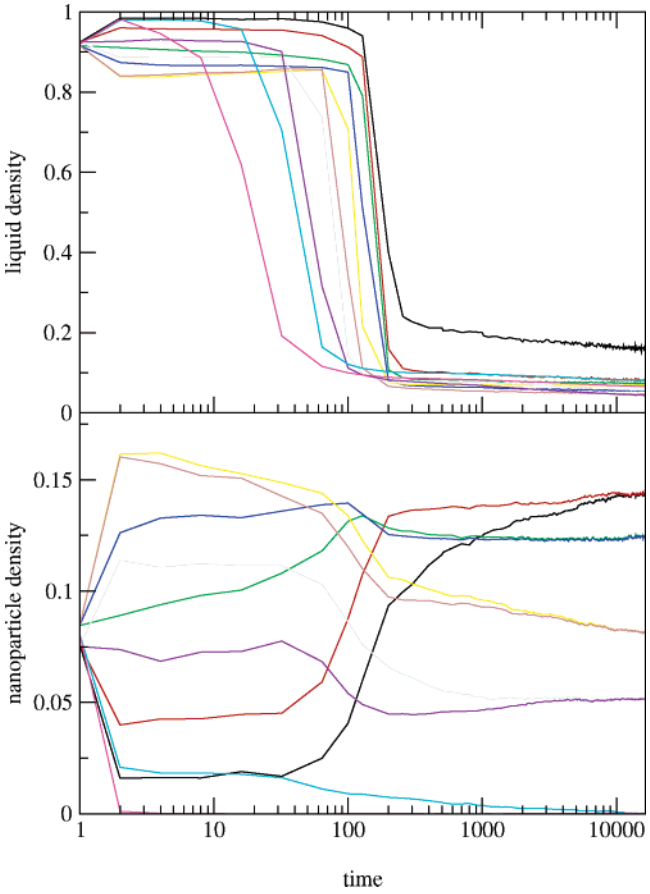

Figure 7. Time evolution of the density of nanoparticles (bottom) and liquid (top) for homogeneous evaporating conditions. At $t = 0$ the interparticle interaction was increased by 25%. Each color represents the time evolution of the 2D density at a different layer. Color scheme same as in Figure 3.

IV. Conclusions

In this paper we have extended the coarse-grained lattice−gas model of Rabani et al.[50] to study drying-mediated self-assembly of nanoparticles in 3D. Unlike the 2D model, our approach explicitly treats the substrate. Furthermore, capillary interactions and solvation forces are treated in the full 3D space.

We find that when the liquid interfacial energy is large, the solvent evaporates gradually layer after layer. The strong solvation forces drive the nanoparticles toward the substrate, forming an effective thin layer of liquid and nanoparticles. Eventually the thin solvent layer completely evaporates, leading to the formation of 2D assembled structures. In this limit the assembly process is well described by the 2D model of Rabani et al.[50] This is true regardless of whether the solvent evaporated homogeneously or heterogeneously in space.

When the solvent wets the boundary of the nanoparticle domains and they remain fluxional, a second small layer of nanoparticles is formed. This is the typical situation when the liquid evaporation is homogeneous in space. In this case full 3D treatment is necessary to describe the formation and growth of this second layer. The size of the second layer also depends on the magnitude of the nanoparticle−substrate interaction. Strong interaction favors the formation of 2D ordered arrays, while weaker interactions results in a small second layer of nanoparticles, similar to the experimental observation. When the liquid evaporation is rather heterogeneous in space and domain edges are not fluxional, the size of the second layer diminishes.

The formation of complex 3D assembled arrays is a challenging task. In this paper we explored one possible route to form nanostalagmites. This occurs when suddenly the nanoparticle−nanoparticle interaction strength is increased relative to that of the liquid−liquid interaction strength. Experimentally, this can be achieved by adding small amounts of a cosolvent with respect to which the nanoparticles are solvophobic or by optically exciting the nanoparticles, thereby increasing their attractions. The formation of the nanostalagmites is strongly coupled to the liquid−vapor phase-transition. Furthermore, the shape of the stalagmites is conical with dimensions that depend mainly on the diffusion rate of nanoparticles.

Several new directions can be studied within the present 3D model. Since the substrate is treated explicitly, effects such as substrate roughness and substrate patterning can be addressed directly. Furthermore, other evaporation scenarios may lead to exotic 3D morphologies. For example, density fluctuations near a critical point may lead to the formation of interesting 3D self-assembled structures governed by the long wavelength fluctuations of the solvent. These and other issues are currently under investigation.

Acknowledgment. This work is dedicated to the occasion of David Chandler's 60th birthday. Some of his pioneering contribution in statistical mechanics is touched upon in this work. It is an honor for us to dedicate this work to him. We thank Haim Diamant for stimulating discussion. This work was supported by the US-Israel Binational Science Foundation (grant number 2002100).

References and Notes

(1) Heath, J. R. *Science* **1995**, *270*, 1315.
(2) Collier, C. P.; Vossmeyer, T.; Heath, J. R. *Annu. Rev. Phys. Chem.* **1998**, *49*, 371.
(3) Andres, R. P.; Bielefeld, J. D.; Henderson, J. I.; Janes, D. B.; Kolagunta, V. R.; Kubiak, C. P.; Mahoney, W. J.; Osifchin, R. G. *Science* **1996**, *273*, 1690−1693.
(4) Korgel, B. A.; Fitzmaurice, D. *Phys. Rev. Lett.* **1998**, *80*, 3531.
(5) Motte, L.; Billoudet, F.; Pileni, M. P. *J. Phys. Chem.* **1995**, *99*, 16425−16429.
(6) Harfenist, S. A.; Wang, Z. L.; Alvarez, M. M.; Vezmar, I.; Whetten, R. L. *J. Phys. Chem.* **1996**, *100*, 13904−13910.
(7) Korgel, B. A.; Fullam, S.; Connolly, S.; Fitzmaurice, D. *J. Phys. Chem. B* **1998**, *102*, 8379.
(8) Sear, R. P.; Chung, S. W.; Markovich, G.; Gelbart, W. M.; Heath, J. R. *Phys. Rev. E* **1999**, *59*, R6255−R6258.
(9) Petit, C.; Taleb, A.; Pileni, M. P. *Adv. Mater.* **1998**, *10*, 259.
(10) Sun, S.; Murray, C. B. *J. Appl. Phys.* **1999**, *85*, 4325.
(11) Puntes, V. F.; Krishnan, K. M.; Alivisatos, A. P. *Science* **2001**, *291*, 2115.
(12) Ziegler, K. J.; Doty, R. C.; Johnston, K. P.; Korgel, B. A. *J. Am. Chem. Soc.* **2001**, *123*, 7797.
(13) Colvin, V. L.; Goldstein, A. N.; Alivisatos, A. P. *J. Am. Chem. Soc.* **1992**, *114*, 5221.
(14) Murray, C. B.; Kagan, C. R.; Bawendi, M. G. *Science* **1995**, *270*, 1335−1338.
(15) Ge, G.; Brus, L. E. *J. Phys. Chem B* **2000**, *104*, 9573−9575.
(16) Ge, G.; Brus, L. E. *Nano. Lett.* **2001**, *1*, 219−222.
(17) Ulman, A. *Adv. Mater.* **1993**, *5*, 55−57.
(18) Vossmeyer, T.; Reck, G.; Katsikas, L.; Haupt, E. T. K.; Schulz, B.; Weller, H. *Science* **1995**, *267*, 1476.
(19) Mićić, O. I.; Jones, K. M.; Cahill, A.; Nozik, A. J. J. *Phys. Chem. B* **1998**, *102*, 9791.
(20) Fried, T.; Shemer, G.; Markovich, G. *Adv. Matt.* **2001**, *13*, 1158−1161.
(21) Tang, J.; Ge, G.; Brus, L. E. *J. Phys. Chem. B* **2002**, *106*, 5653−5658.
(22) Gelbart, W. M.; Sear, R. P.; Heath, J. R.; Chaney, S. *Faraday Discuss.* **1999**, *112*, 299−307.
(23) Whitesides, G. M.; Grzybowski, B. *Science* **2002**, *295*, 2418−2421.
(24) Freeman, R. G.; Grabar, K. C.; Allison, K. L.; Bright, R. M.; Davis, J. A.; Guthrie, A. P.; Hommer, M. B.; Jackson, M. A.; Smith, P. C.; Walter, D. G.; Natan, M. J. *Science* **1995**, *267*, 1629−1632.
(25) Rabani, E.; Egorov, S. *J. Chem. Phys.* **2001**, *115*, 3437.

(26) Rabani, E.; Egorov, S. *Nano Lett.* **2002**, *2*, 69.
(27) Rabani, E.; Egorov, S. *J. Phys. Chem. B* **2002**, *106*, 6771−6778.
(28) Egorov, S. A. *Phys. Rev. E* **2004**, *70*, 031402.
(29) Patel, N.; Egorov, S. A. *J. Chem. Phys.* **2004**, *121*, 4987−4997.
(30) Saunders, A. E.; Shah, P. S.; Park, E. J.; Lim, K. T.; Johnston, K. P.; Korgel, B. A. *J. Phys. Chem. B* **2004**, *108*, 15969−15975.
(31) Elbaum, M.; Lipson, S. G. *Phys. Rev. Lett.* **1994**, *72*, 3562−3565.
(32) Lin, X. M.; Jaeger, H. M.; Sorensen, C. M.; Klabunde, K. J. *J. Phys. Chem. B* **2001**, *105*, 3353−3357.
(33) Deegan, R. D.; Bakajin, O.; Dupont, T. F.; Huber, G.; Nagel, S. R.; Witten, T. A. *Nature* **1997**, *389*, 827−830.
(34) Ohara, P. C.; Leff, D. V.; Heath, J. R.; Gelbart, W. M. *Phys. Rev. Lett.* **1995**, *75*, 3466−3469.
(35) Luedtke, W. D.; Landman, U. *J. Phys. Chem.* **1996**, *100*, 13323.
(36) Alder, B. J.; Wainwright, T. E. *J. Chem. Phys.* **1957**, *27*, 1208.
(37) Hamaker, H. C. *Physica* **1937**, *4*, 1058.
(38) Seul, M.; Wolfe, R. *Phys. Rev. A* **1992**, *46*, 7519−7533.
(39) Seul, M.; Wolfe, R. *Phys. Rev. A* **1992**, *46*, 7534−7547.
(40) Seul, M.; Andelman, D. *Science* **1995**, *267*, 476−483.
(41) Jang, J.; Oh, J. H. *Chem. Commun.* **2002**, *19*, 2200.
(42) Jang, J.; Oh, J. H. *Langmuir* **2004**, *20*, 8419−8422.
(43) Ohara, P. C.; Heath, J. R.; Gelbart, W. M. *Angew. Chem., Int. Ed.* **1997**, *36*, 1078.
(44) Ohara, P. C.; Gelbart, W. M. *Langmuir* **1998**, *14*, 3418−3424.
(45) Maillard, M.; Motte, L.; Ngo, A. T.; Pileni, M. P. *J. Phys. Chem. B* **2000**, *104*, 11871−11877.
(46) Stowell, C.; Korgel, B. A. *Nano Lett.* **2001**, *1*, 595−600.
(47) Binder, K. Phase transformation in materials. In *Material science and technology*; Haasen, P., Ed.; VCH: Weinham, 1990; Vol. 5.
(48) Hohenberg, P. C.; Halperin, B. I. *Rev. Mod. Phys.* **1977**, *49*, 435−479.
(49) Bray, A. J. *Adv. Phys.* **2002**, *51*, 481−587.
(50) Rabani, E.; Reichman, D. R.; Geissler, P. L.; Brus, L. E. *Nature* **2003**, *426*, 271−274.
(51) Rabani, E. *J. Chem. Phys.* **2001**, *115*, 1493.
(52) Rabani, E. *J. Chem. Phys* **2002**, *116*, 258.
(53) TenWolde, P. R.; Sun, S. X.; Chandler, D. *Phys. Rev E* **2001**, *65*, 011201.
(54) TenWolde, P. R.; Chandler, D. *Proc. Natl. Acad. Sci. U.S.A.* **2002**, *99*, 6539−6543.
(55) Maibaum, L.; Chandler, D. *J. Phys. Chem. B* **2003**, *107*, 1189−1193.
(56) Chandler, D. *Introduction to Modern Statistical Mechanics*; Oxford: New York, 1987.
(57) To mimic realistic experimental situations, one has to scale ϵ_n such that the overall nanoparticle interactions increase with increasing nanoparticle diameter $\epsilon_n \propto d^{-1}$, where d is the diameter of the nanoparticles.